A TABLE OF GENUS TWO HANDLEBODY-KNOTS WITH SEVEN CROSSINGS

GIOVANNI BELLETTINI, GIOVANNI PAOLINI, MAURIZIO PAOLINI, AND YI-SHENG WANG

Abstract. We enumerate all genus two handlebody-knots with seven crossings, up to mirror image, extending the Ishii-Kishimoto-Moriuchi-Suzuki table. Table 1 lists all irreducible handlebody-knots with seven crossings (69 entries). Table 2 lists all reducible handlebody-knots (9 entries).

1. Introduction

A *genus g handlebody-knot* is an embedded handlebody V of genus g in the oriented 3-sphere $\mathbb{S}^3$, and a *spatial graph* is an embedded finite connected graph Γ in $\mathbb{S}^3$. A spine of a handlebody-knot is a spatial graph, and a regular neighborhood of a spatial graph is a handlebody-knot. While every spatial graph has a unique regular neighborhood, up to isotopy, a handlebody-knot can have infinitely many different spines. Two handlebody-knots V, V' (resp. spatial graphs Γ, Γ') are *equivalent* if there is an orientation-preserving self-homeomorphism of $\mathbb{S}^3$ sending V to V' (resp. sending Γ to Γ'); if the condition "orientation-preserving" is dropped, we say they are *equivalent, up to mirror image*. The *crossing number* of a handlebody-knot V is the minimum of the crossing numbers of all its spines. A handlebody-knot V is *irreducible* if there exists no 2-sphere in $\mathbb{S}^3$ meeting V at an essential disk of V.

Ishii-Kishimoto-Moriuchi-Suzuki [10, Table 1] enumerates, up to mirror image, all irreducible genus two handlebody-knots up to six crossings. Our main result extends their table to seven crossing genus two handlebody-knots.

Theorem 1.1. *Table* 1 *enumerates all irreducible genus two handlebody-knots with seven crossings, up to mirror image.*

The construction of Table 1 allows us to obtain a table of reducible handlebody-knots, extending [10, Table 4].

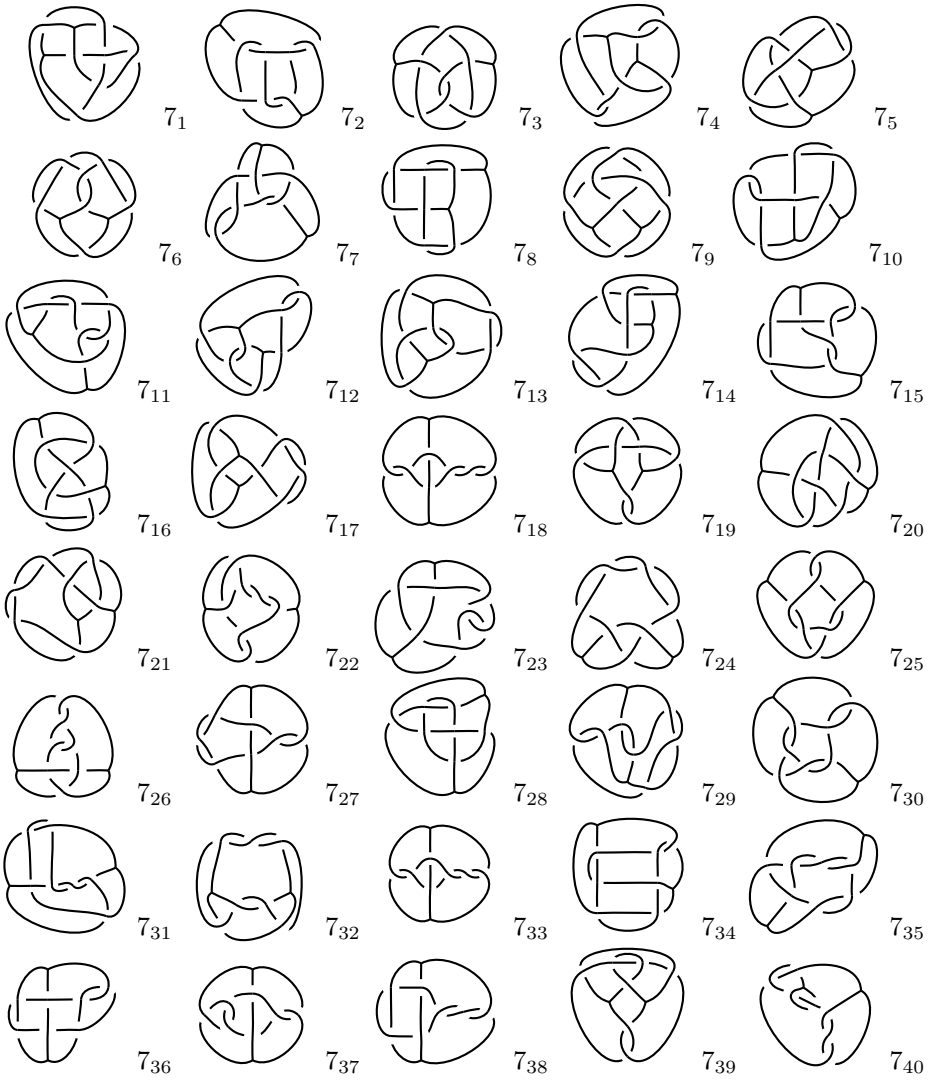
Theorem 1.2. *Table* 2 *enumerates all reducible genus two handlebody-knots with seven crossings, up to mirror image.*

Proof. The classification of $\mathcal{D}$ in Section 3 produces Tables 1 and 2; the entries of Table 2 are reducible by construction, while those of Table 1 are irreducible by Corollary 5.2. □

The paper is structured so that the completeness of the two tables is given in Section 3, while in Sections 4 and 6, we prove that there are no duplications in Tables 1, 2. Section 5 explains how the irreducibility of handlebody-knots in Table 1 is obtained.

Date: September 30, 2026.
2020 *Mathematics Subject Classification.* 57K12, 57M15, 05C30 .
Key words and phrases. handlebody-knot table, spatial graphs.

TABLE 1. Irreducible genus two handlebody-knots with seven crossings (continued on next page).



2. PRELIMINARIES

2.1. **Diagrams.** Given a spatial graph Γ and $p \in \mathbb{S}^3 - \Gamma$, then we say a projection $\pi : \mathbb{S}^3 - \{p\} \simeq \mathbb{R}^3 \to \mathbb{R}^2$ is *regular* with respect to Γ if π is in general position [23] (see [7, Section 4.4]). In particular, the image $\pi(\Gamma)$ is a plane graph with vertices the union of double points of π and vertices of Γ.

Given a regular projection π with respect to Γ, a *diagram* of Γ is given by replacing each double point in $\pi(\Gamma)$ with a *crossing*, where the broken arc corresponds to the edge of Γ underneath the edge the unbroken arc corresponds to in $\mathbb{R}^3 \simeq \mathbb{S}^3 - \{p\}$; see Fig. 2.1a. A *diagram* of a handlebody-knot V is a diagram of one of its spines. The plane graph $\pi(\Gamma)$ is called *the underlying graph* of the diagram.

The *crossing number* of a diagram of a spatial graph Γ (resp. handlebody-knot V) is the number of the crossings the diagram has. The *crossing number* $c(\Gamma)$ of Γ (resp. $c(V)$ or V) is the minimum of the crossing numbers over all diagrams of Γ

TABLE 1. (continued)

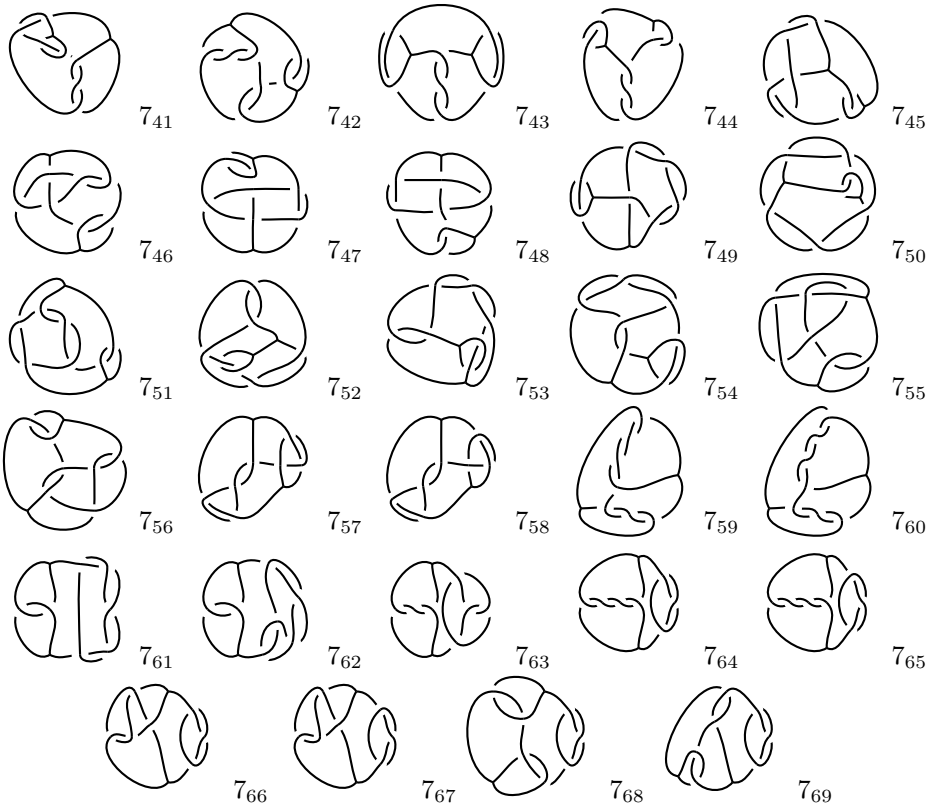
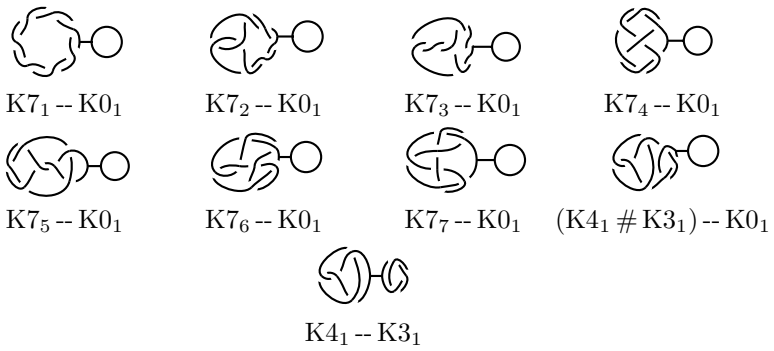


TABLE 2. Reducible handlebody-knots with seven crossings.



(resp. V). A diagram of Γ (resp. V) that attains the crossing number of Γ (resp. V) is called a *minimal diagram*. A minimal diagram of Γ is in general not unique.

Given a diagram D of a spine Γ of a handlebody-knot V, observe that if $v \in D$ is a vertex of valence greater than 3 and $\mathcal{N}(v) \subset \mathbb{R}^2$ is a regular neighborhood of v with $D_v := D \cap \mathcal{N}(v)$ a deformation retract of $\mathcal{N}(v)$, then we can replace D_v with a new graph $\tilde{D}_v$ where $\tilde{D}_v \cap \partial\mathcal{N}(v) = D_v \cap \partial\mathcal{N}(v)$ and all vertices of $\tilde{D}_v$ in the interior of $\mathcal{N}(v)$ are trivalent; see Fig. 2.1b. In particular, every handlebody-knot has a minimal diagram which is a diagram of a trivalent spine—namely, all vertices are trivalent.



(a) Turning 4-valent vertices into crossings. (b) Turning into trivalent vertices.

FIGURE 2.1

A trivalent spine of a genus g handlebody-knot has $2g-2$ trivalent vertices. Therefore, a trivalent spine of a genus two handlebody-knot is either a spatial theta graph or a spatial handcuff graph. For the sake of simplicity, hereinafter, a minimal diagram always refers to a minimal diagram of a trivalent spatial graph or a trivalent spine of a handlebody-knot.

Recall that the *edge-connectivity* of a graph is the minimum number of edges whose deletion disconnects the graph. A graph is e-connected if it has edge-connectivity greater than or equal to e. A diagram of a spatial graph is said to have *connectivity* e (resp. to be *e-connected*) if its underlying graph has edge-connectivity e (resp. is e-connected).

To study handlebody-knots in terms of their diagrams, we recall that *generalized Reidemeister moves* are the local changes depicted in Figs. 2.2 and 2.3 and an *IH-move* is the local change in Fig. 2.4.

Theorem 2.1 ([9, Corollary 2])**.** *Two handlebody-knots are equivalent if and only if their diagrams are related by a finite sequence of generalized Reidemeister moves and IH-moves.*

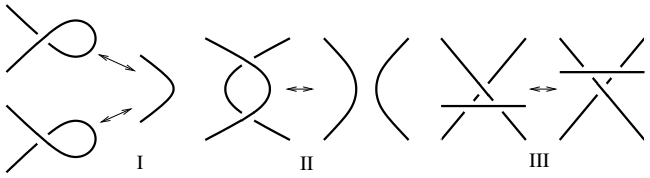


FIGURE 2.2. Classical Reidemeister moves of type I, II, III.

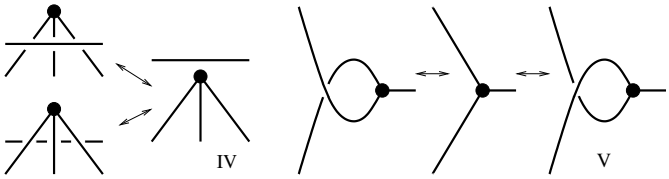


FIGURE 2.3. Reidemeister moves IV and V involving a trivalent vertex.

3. Completeness

Hereinafter, for the sake of simplicity, unless otherwise specified, by a handlebody-knot, we understand a genus two handlebody-knot. To enumerate all seven crossing handlebody-knots, our approach is to divide minimal diagrams into three classes:

(1) 3-connected minimal diagrams;
(2) Minimal diagrams with connectivity 2;
(3) Minimal diagrams with connectivity 1.

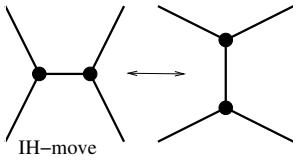


FIGURE 2.4. IH-move.

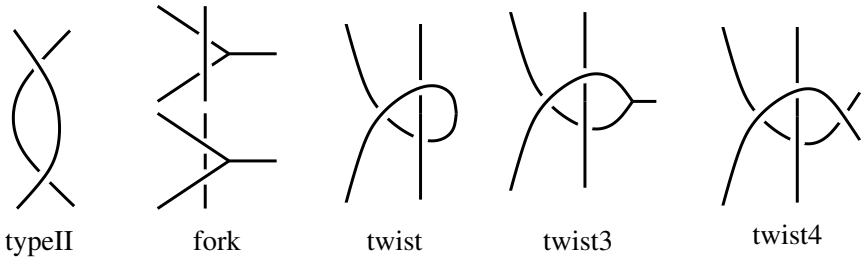


FIGURE 3.1. Crossing-reducing moves. They consist of a sequence of Reidemeister moves as follows (from left to right): II ; II^{-1} IV ; III I ; III V ; III II . Notation "II^{-1}" means that move II is performed in the "crossing-increasing" direction.

3.1. **3-connected diagrams.** Our goal here is to find all seven crossing handlebody-knots that have a 3-connected minimal diagram. To do so, we first enumerate all 3-connected plane graphs with two trivalent vertices and seven quadrivalent vertices, and then replace each quadrivalent vertex with a crossing.[1] The first part is done by a code devised by the second author, and it results in 908 such plane graphs, up to mirror image. Since, for each quadrivalent vertex, there are two possible choices of crossings (see Fig. 2.1a), these 908 plane graphs produce an unmanageable number, $908 \cdot 2^6$, of diagrams, up to mirror image, where we take advantage of the freedom to revert all crossings to fix the overcrossing choice of one of the vertices arriving at the exponent $6 = 7 - 1$. To reduce the number of diagrams, a software developed by the third author is implemented to drop diagrams that

- represent a handlebody-link with more than one component, or
- is recognized to be nonminimal via moves in Figs. 3.1 and 3.2.

In addition, one choice is selected for any pair of over/under crossings

- that results in embeddings having a portion depicted in Fig. 3.3 or
- that are directly connected by an IH move (Fig. 2.4).

Consequently, we obtain a refined set $\mathcal{D}_3$ of 808 diagrams, where, for every seven crossing handlebody-knot V with a 3-connected minimal diagram, there is a minimal diagram in $\mathcal{D}_3$ representing V. We arrive at the final number of 808 in two steps, first all situations depicted in Figures 3.1 and 3.2 with the exception of the IH+V move are recognized by the `appcontour` software and used to generate a set of 1632 diagrams. This set is then reduced to 808 entries by automatically recognizing situations matching the move "IH+V" of Figure 3.2 and, for any pair of diagrams that are directly connected by an IH move only one is retained.

[1]Note that the Whitney theorem [22] is not applicable here since a 3-connected graph may not be 3-vertex-connected.

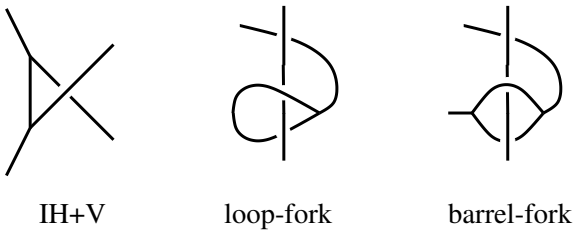


FIGURE 3.2. More crossing-reducing moves. "IH+V" is an IH-move followed by a V move (Fig. 2.3); "loop-fork" and "barrel-fork" are performed by twisting the loop/barrel (see Fig. 3.3) and then applying the fork move (Fig. 3.1).

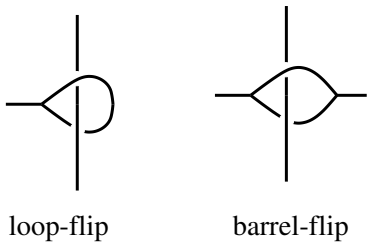


FIGURE 3.3. Loop/barrel flipping moves. They consist of the following sequence of Reidemeister moves "loop-flip": II^{-1} V III I resulting in a reversal of the two overcrossings. "barrel-flip": same sequence as for "loop-flip" with a V move replacing I, also resulting in a reversal of the overcrossings.

The filtering process described by the four items above does not guarantee against nonminimal diagrams and they must be manually uncovered during the *dynamic process* described in Section 4.1. To this aim it greatly helps to include in the process also the handlebody-knots with fewer than 7 crossings, for which we have a complete list. Indeed, a nonminimal 7-crossings diagram must be indistinguishable by any invariant against some handlebody-knot with fewer crossings raising the suspicion that it is actually equivalent to it. If we are not able to manually prove equivalence, the alternative is that it is actually minimal and we are dealing with a *hard-pair* for which we must manually prove inequivalence. Indeed we have two hard-pairs where one entry has fewer crossings (see Section 4.1).

Concerning the exclusion of handlebody-links we observe that the number of components of a diagram does not depend on the way we chose the overpasses at crossings and can be easily computed in an automated way.

In [3] we provide details for the sets described here, in particular the list of diagrams in set $\mathcal{D}_3$, file `D3.csv`.

3.2. **Diagrams with connectivity 2.** The aim here is to find all seven crossing handlebody-knots that have a minimal diagram with connectivity 2 and no minimal diagram with connectivity 1.

2-sum of diagrams and spatial graphs. A 2-sum of two spatial graphs Γ_1, Γ_2 is constructed as follows [14]: For each i, choose an edge e_i in Γ_i; secondly, consider

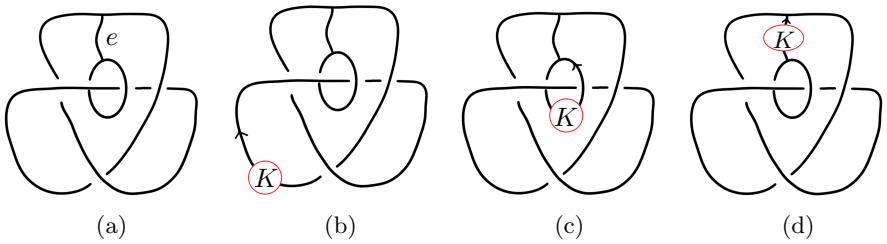


FIGURE 3.4. 2-sum.

a 3-ball B_i with $B_i \cap \Gamma_i = B_i \cap e_i$; thirdly, orient e_i so that e_i is going out of B_i at a point $a_i \in e_i \cap \partial B_i$ and going in B_i at a point $b_i \in e_i \cap \partial B_i$. Then the *order*-2 *vertex connected sum*, abbreviated to 2-*sum*, is the spatial graph given by gluing the exteriors $E(B_1)$ and $E(B_2)$ with an orientation-reversing homeomorphism $h : \partial E(B_1) \to \partial E(B_2)$ with $h(a_1) = b_2$, $h(b_1) = a_2$. The spatial graphs Γ_1, Γ_2 are called *summands* of the 2-sum.

Since a 2-sum depends on the choice of edges in Γ_i and a given orientation, it is not unique; for instance, Figs. 3.4b, 3.4c, 3.4d illustrate three different 2-sums of an oriented knot K and the spatial graph in Fig. 3.4a. If K is not invertible, then two different orientations of the edge e in Fig. 3.4a yield two different 2-sums.

We denote by $\Gamma_1 \# \Gamma_2$ the set of all possible 2-sums of Γ_1 or its mirror image and Γ_2 or its mirror image.

Given a *diagram* D of a handlebody-knot V, a prime factor $N \subset \mathbb{R}^2$ of D is a disk N with ∂N meeting D at two points a, b such that $N \cap D$ together with an arc outside N is a diagram of a prime knot K, called the *induced prime knot*. A *system* $\mathcal{N}$ of prime factors is a set of mutually disjoint prime factors, and it is *maximal* if it is not a proper subset of another system of prime factors.

Given a system $\mathcal{N} = \{N_1, \cdots, N_k\}$ of prime factors, let α_i be an arc in N_i with $\partial \alpha_i = D \cap \partial N_i$, then $\big(D - (N_1 \cup \cdots \cup N_k)\big) \cup (\alpha_1 \cup \cdots \cup \alpha_k)$ is a diagram D_0 of a spatial handcuff or theta graph Γ_0; D_0 and Γ_0 are called the *base diagram* and *base graph*, respectively. The spatial graph D represents can thus be regarded as a 2-sum of Γ_0 and some prime knots.

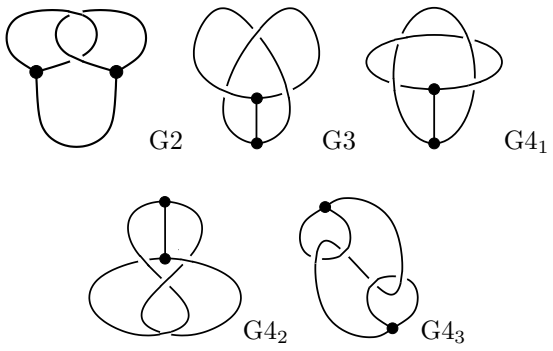
Suppose D is minimal with 7 crossings and connectivity 2. Then D admits a non-empty maximal system $\mathcal{N} = \{N_1, \cdots, N_k\}$ of prime factors—its existence follows from the induction on the number of crossings, and the base graph D_0 is minimal and 3-connected, given $\mathcal{N}$ is maximal. Since D has only 7 crossings and a non-trivial knot has at least 3 crossings, we have $k \leq 2$, namely,

$$\Gamma \in (\Gamma_0 \# K_1) \text{ or } \Gamma \in (\Gamma_0 \# K_1) \# K_2$$

where K_1, K_2 are the prime knots induced by N_1, N_2, respectively. The base graph Γ_0 cannot be a trivial spatial handcuff since V admits no minimal diagram with connectivity 1. If Γ_0 is a trivial spatial θ-graph, then, since $k \leq 2$, there is an edge in D joining the two trivalent vertices. Applying an IH-move along the edge turns D into a diagram with connectivity 1 without changing the number of crossings, contradicting our assumption. As a result, the base graph Γ_0 is non-trivial, and hence D_0 has at least two crossings. This implies $k = 1$, and K_1 has at most five crossings, and Γ_0 has at most four crossings.

Since prime knots up to five crossings are all invertible, the set $\Gamma_0 \# K_1$ contains at most six elements, depending on the arc in Γ_0 where the 2-sum is performed and the chirality of K_1. Note that handlebody-knots so produced might not have seven crossings.

TABLE 3. Spatial graphs up to four crossings. G2 and $G4_1$ are handcuff graphs and correspond respectively to 2_1 and 4_1 of [15, Table 1]; $G4_3$ is a nonprime handcuff graph obtained as the 3-sum of two copies of entry 2_1 in [15]; G3 and $G4_2$ are theta-curves corresponding respectively to 3_1 and 4_1 of [14, Fig. 1].



To determine Γ_0, we note that, since D_0 is 3-connected, it suffices to enumerate all spatial graphs that have a 3-connected minimal diagram, up to four crossings. This is done by the code developed by the second author, which allows us to find all 3-connected plane graphs with two trivalent vertices and up to four quadrivalent vertices. Such spatial graphs are enumerated in Table 3 (see [1, Table 4] and [14, 15]). Denote by Kn_m the prime knot n_m in the knot table. Then, since Γ_0 is in Table 3, seven crossing handlebody-knots V that have a minimal diagram with connectivity 2 but no minimal diagram with connectivity 1 can be enumerated as follows.

- $\mathrm{G2}\,\#\,\mathrm{K3}_1$: the handlebody-knot 5_4 of [10, Table 1];
- $\mathrm{G3}\,\#\,\mathrm{K3}_1$: the handlebody-knots 6_{14} and 6_{15} of [10, Table 1].
- $\mathrm{G2}\,\#\,\mathrm{K4}_1$: the handlebody-knot 6_{16} of [10, Table 1];
- $\mathrm{G2}\,\#\,\mathrm{K5}_1$: the handlebody-knot 7_{61} of Table 1;
- $\mathrm{G2}\,\#\,\mathrm{K5}_2$: the handlebody-knot 7_{62} of Table 1;
- $\mathrm{G3}\,\#\,\mathrm{K4}_1$: the handlebody-knot 7_{63} of Table 1;
- $\mathrm{G4}_1\,\#\,\mathrm{K3}_1$: the handlebody-knots 7_{64} and 7_{65} of Table 1
- $\mathrm{G4}_2\,\#\,\mathrm{K3}_1$: the handlebody-knots 7_{66} and 7_{67} of Table 1.
- $\mathrm{G4}_3\,\#\,\mathrm{K3}_1$: the handlebody-knots 7_{68} and 7_{69} of Table 1.

Each handlebody-knot above admits a canonical diagram with a single prime factor associated to a minimal diagram of Kn_m; see Table 1. The set of diagrams is denoted by $\mathcal{D}_2$ and contains 14 entries, listed in [3], file `D2.csv`. It is obtained as follows: first we construct all the embeddings (with no overpass information) matching the list above restricted to 7-crossings (six entries). With the exception of $G4_3$ we must obstruct the IH move that would otherwise lead to nonminimality. Since we lose, at this stage, the overcrossing information we can forget about the chirality of each factor obtaining exactly one embedding for five of these six entries. The entry $\mathrm{G4}_3\,\#\,\mathrm{K3}_1$ contributes two distinct (flattened) embeddings, they are distinguished by the choice of the arc in $G4_3$, two possibilities since we can exchange the two loops. We also add two different embeddings of these latter two realizations of $\mathrm{G4}_3\,\#\,\mathrm{K3}_1$. This is done just to be on the safe side, since we know in advance (and we verified a-posteriori) that we obtain equivalent (up to mirror image) diagrams. This set of 9 embeddings will then produce the 14 pairings with a choice of the overpass information after dropping trivially nonminimal choices. This is summarized in Table 4.

TABLE 4. 2-sums with seven crossings. The second column shows the number of possibly inequivalent flattened (no overcrossing information) embeddings. The third column shows the number of corresponding diagrams that are not trivially nonminimal. The fourth column is the reference number in list `D2.csv` of [3]. The numbers in the last row could be safely reduced to the numbers in parentheses.

name	**# fl.emb.**	**# diag.**	**ref.**
$G2\#K5_1$	1	1	909
$G2\#K5_2$	1	1	910
$G3\#K4_1$	1	2	911
$G4_1\#K3_1$	1	2	912
$G4_2\#K3_1$	1	2	913
$G4_3\#K3_1$	4(2)	6(3)	914–917
total	9	14	

3.3. **Diagrams with connectivity 1.** The aim here is to find all seven crossing handlebody-knots that have a minimal diagram with connectivity 1.

1-sum of handlebody-knots. Let V_1, V_2 be two handlebody-knots of genus g_1, g_2, respectively. Then the 1-sum $V_1 \text{ -- } V_2$ is constructed as follows: For each $i = 1, 2$, choose a 3-ball B_i such that $D_i := V_i \cap B_i = \partial V_i \cap \partial B_i$ is a disk. Let $h : \partial E(B_1) \to \partial E(B_2)$ be an orientation-reversing homeomorphism with $h(D_1) = D_2$. Then $V_1 \text{ -- } V_2$ is the genus $g_1 + g_2$ handlebody-knot obtained by gluing $D_1 \subset V_1$ to $D_2 \subset V_2$ via h in the 3-sphere $E(B_1) \cup_h E(B_2)$; see Fig. 3.5.

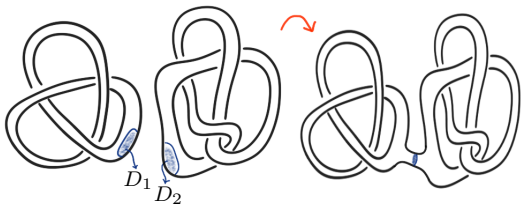


FIGURE 3.5. One sum of $K3_1$ and $K4_1$.

Enumeration. Suppose the handlebody-knot V has a minimal diagram D with connectivity 1, and let $e \in D$ be the edge cutting which disconnects D. Then $D - \{e\}$ consists of two components D_1, D_2. By the minimality of D, the diagrams D_1, D_2 are minimal. Also, if V_1, V_2 are the genus one handlebody-knots represented by D_1, D_2, then D is a diagram of $V_1 \text{ -- } V_2$, equivalent to V. Therefore, to enumerate handlebody-knots with a minimal diagram of connectivity 1, it suffices to consider all one sums $V_1 \text{ -- } V_2$ with V_1, V_2 of genus one and $c(V_1) + c(V_2) = 7$. Since a genus one handlebody-knot is equivalent to a knot, we use the same notation Kn_m to denote the genus one handlebody-knot corresponding to the prime knot Kn_m, and let $K0_1$ be the trivial genus one handlebody-knot.

- $K7_1 \text{ -- } K0_1$;
- $K7_2 \text{ -- } K0_1$;
- $K7_3 \text{ -- } K0_1$;
- $K7_4 \text{ -- } K0_1$;
- $K7_5 \text{ -- } K0_1$;
- $K7_6 \text{ -- } K0_1$;

- $\mathrm{K7}_7$ -- $\mathrm{K0}_1$;
- $\mathrm{K4}_1$ -- $\mathrm{K3}_1$;
- $(\mathrm{K4}_1 \# \mathrm{K3}_1)$ -- $\mathrm{K0}_1$.

For each handlebody-knot above, there is a canonical diagram given by minimal diagrams of Kn_m as shown in Table 2; the set of diagrams is denoted by $\mathcal{D}_1$.

3.4. **Conclusion.** Let $\mathcal{D} = \mathcal{D}_1 \cup \mathcal{D}_2 \cup \mathcal{D}_3$.

Theorem 3.1 (Completeness)**.** *For every seven crossing handlebody-knot V, there is a minimal diagram in $\mathcal{D}$ representing V.*

Proof. As shown in Section 3.3, if V has a minimal diagram with connectivity 1, then $\mathcal{D}_1$ contains a minimal diagram of V. Suppose V has no minimal diagram with connectivity 1. If V has a minimal diagram with connectivity 2, Section 3.2 implies $\mathcal{D}_2$ contains a minimal diagram of V; otherwise V has a minimal diagram in $\mathcal{D}_3$; see Section 3.1. □

Remark 3.1. In general, it is not known whether the minimal diagram of a 1-sum always has connectivity 1. Similarly, it is unclear whether a minimal diagram of a handlebody-knot having a spine that is a 2-sum always has connectivity 2.

The enumeration is, however, based on the connectivity of minimal diagrams, and not on the decomposition type of handlebody-knots, and therefore does not depend on the aforementioned open problems. For instance, if a 1-sum has no minimal diagrams with connectivity 1, then its minimal diagram(s) can be found in $\mathcal{D}_2 \cup \mathcal{D}_3$.

Remark 3.2. Recall that a spatial graph Γ is *prime* if, for any 3-ball B with ∂B meeting Γ transversally at less than or equal to 3 points, the intersection $B \cap \Gamma$ is contained in a proper disk in B; see [14], [15]. In particular, if Γ has a diagram with connectivity less than or equal to 3, then Γ cannot be prime. Tables of prime spatial handcuff graphs and θ-graphs, up to seven crossings, are given in Moriuchi [14], [15], [16]. Denote by $\mathcal{G}$ the set of Moriuchi's spatial graphs, up to equivalence and mirror image; there are 134 in total, and let $\mathcal{H}$ be the set of genus two handlebody-knots with up to seven crossings, up to equivalence and mirror image; 90 of them are irreducible. Consider the function

$$\mathcal{N} : \mathcal{G} \to \mathcal{H}$$

given by taking a regular neighborhood of a spatial graph (see Table 5). Then a natural question arises as to what the image of $\mathcal{N}$ is. Applying the IH-move shows that among all spatial θ-graphs with seven crossings in [14], from 7_{25} onward, all except $7_{40}, 7_{48}, 7_{58}, 7_{60}, 7_{64}$, are non-minimal as a diagram of a handlebody-knot. Similarly, among all spatial handcuff graphs with seven crossings in [15], from 7_{18} onward, all except 7_{21}, are non-minimal as a diagram of a handlebody-knot. On the other hand, those who are minimal, as a diagram of a handlebody-knot, often represent equivalent handlebody-knots, up to mirror image. More precisely,

- spatial θ-graphs $7_{21}, 7_{60}$ in [14] and spatial handcuff graph 7_{21} in [15] represent the handlebody-knot 7_{36} in Table 1;
- spatial θ-graphs $7_{18}, 7_{48}, 7_{58}$ in [14] represent the handlebody-knot 7_{52} in Table 1;
- spatial θ-graph 7_{16} in [14] and spatial handcuff graph 7_{17} in [15] represent the handlebody-knot 7_{32} in Table 1.

In summary, there are 28 handlebody-knots of seven crossings in Table 1 that are not in the image of $\mathcal{N}$, namely, all handlebody-knots from 7_{40} onward except $7_{47}, 7_{52}$. Particularly, none of their seven-crossing spines is prime.

TABLE 5. Map $\mathcal{N}$. We omit graphs that are mapped to the trivial $K0_1$ -- $K0_1$ handlebody-knot. The numbering for θ-graphs (first table) and handcuff graphs (second table) refers to [14, Fig. 1] and [15, Fig. 1] respectively. The numbering for handlebodies ('h.body' columns) is taken from Table 1 and [10, Table 1]

θ-graph	h.body	θ-graph	h.body	θ-graph	h.body
5_1	5_3	7_{10}	7_{26}	7_{35}	5_2
5_2	5_2	7_{11}	7_{27}	7_{39}	5_2
6_1	6_8	7_{12}	7_{28}	7_{40}	7_{47}
6_2	6_9	7_{13}	7_{29}	7_{41}	6_{12}
6_3	6_{12}	7_{14}	7_{30}	7_{45}	6_{13}
6_4	6_{13}	7_{15}	7_{31}	7_{47}	6_6
6_7	4_1	7_{16}	7_{32}	7_{48}	7_{52}
6_{11}	5_1	7_{17}	7_{33}	7_{51}	6_{11}
6_{15}	5_1	7_{18}	7_{52}	7_{52}	6_8
7_1	7_{17}	7_{19}	7_{34}	7_{54}	6_2
7_2	7_{18}	7_{20}	7_{35}	7_{55}	6_5
7_3	7_{19}	7_{21}	7_{36}	7_{58}	7_{52}
7_4	7_{20}	7_{22}	7_{37}	7_{60}	7_{36}
7_5	7_{21}	7_{23}	7_{38}	7_{61}	6_9
7_6	7_{22}	7_{24}	7_{39}	7_{62}	5_2
7_7	7_{23}	7_{26}	6_{13}	7_{64}	7_{47}
7_8	7_{24}	7_{30}	6_2		
7_9	7_{25}	7_{31}	5_2		

h. graph	h.body	h. graph	h.body	h. graph	h.body
6_1	6_7	7_6	7_6	7_{17}	7_{32}
6_2	6_4	7_7	7_7	7_{20}	5_3
6_3	6_3	7_8	7_8	7_{21}	7_{36}
6_4	6_2	7_9	7_9	7_{24}	4_1
6_6	5_2	7_{10}	7_{10}	7_{25}	6_8
6_9	5_2	7_{11}	7_{11}	7_{27}	5_3
7_1	7_1	7_{12}	7_{12}	7_{29}	6_5
7_2	7_2	7_{13}	7_{13}	7_{31}	6_{12}
7_3	7_3	7_{14}	7_{14}	7_{32}	6_6
7_4	7_4	7_{15}	7_{15}	7_{33}	5_1
7_5	7_5	7_{16}	7_{16}	7_{34}	6_9

4. No duplicates in the table

Our goal is to classify diagrams in $\mathcal{D}$ into several classes, each of which contains only diagrams that represent the same handlebody-knot, up to equivalence and mirror image. Given the sheer size of $\mathcal{D}$, we adopt a dynamic approach to classify diagrams in $\mathcal{D}$.

4.1. **A dynamic approach.** The dynamic approach can be pictured as a growing rooted tree. The end result is a big rooted tree $\mathcal{T}$, which is a dynamic data structure with data attached to each leaf. Specifically, each leaf of $\mathcal{T}$ contains diagrams that represent one or two equivalence classes of handlebody-knots, up to mirror image.

The tree $\mathcal{T}$ is grown from the degenerate tree with a single vertex, the root, containing all diagrams in $\mathcal{D}$. At start, we apply some weak but computationally efficient invariant t_1 to handlebody-knots represented by diagrams in the root. The diagrams in $\mathcal{D}$ are then divided into classes so that each class contains only diagrams

with the same t_1-invariant. We associate each class with a new leaf connecting to root with an edge, and thus the initial degenerate tree grows into a star. Next, for each leaf v of the star, we apply a slightly stronger invariant t_2, specifically tailored to the leaf v. Thus t_2 divides the diagrams in the leaf v into even smaller classes based on their t_2-invariants. In the same way, we associate each class with a new leaf connecting to v with an edge; note that v is no longer a leaf at this stage. The process repeats itself for each leaf, and whenever we arrive at a stage where the leaf contains only a handful of diagrams or no computationally affordable invariant can distinguish the handlebody-knots the diagrams therein represent, we tag the leaf as *final*. For each final leaf we need to check equivalence of all entries therein. Entries with a higher number of crossings must be checked to be nonminimal. In a few cases, discussed below, we arrive to a partition of the diagrams into two sets of equivalent diagrams that must then be manually shown to be inequivalent (hard pairs). The big tree $\mathcal{T}$ is then the resulting tree, where every leaf is tagged as final; see the web page [19] for a snapshot.

The invariants used here are the Kitano-Suzuki invariants. Given a handlebody-knot V, let G be a finite group; *the Kitano-Suzuki G-invariant* ks_G is the number of conjugate classes of homomorphisms from the fundamental group of the exterior $E(V)$ of V to G; see [12]. When the order of G is small, the computation load of ks_G is rather light, but it grows exponentially as the order of G gets larger. The computational complexity is also highly sensitive to the number of generators in the used presentation of the fundamental group. The finite groups used in our computation are:

- $\mathrm{SL}_2(\mathbb{Z}_p)$ with prime p,
- The symmetric group S_n, $n \in \mathbb{N}$,
- The alternating group A_n, $n \in \mathbb{N}$.

In the process of building the tree $\mathcal{T}$, we start with G of a small size and move on to larger ones.

The invariant ks_G depends only on the exterior of a handlebody-knot, so it cannot differentiate inequivalent handlebody-knots with homeomorphic exteriors; such handlebody-knots, however, abound [17], [13], [4]. A stronger invariant, the *G-image* invariant introduced in [4] is thus used. The *G-image* invariant is constructed as follows: Consider the homomorphisms

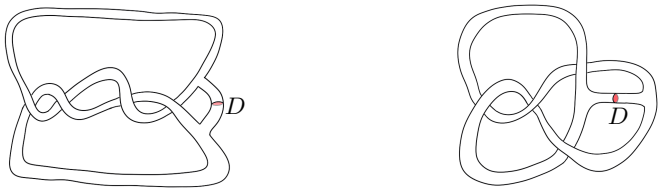
$$\iota_{1*} : \pi_1(\partial V) \to \pi_1(V), \quad \iota_{2*} : \pi_1(\partial V) \to \pi_1(E(V))$$

induced by the inclusions $\iota_1 : \partial V \to V$ and $\iota_2 : \partial V \to E(V)$. Then a surjective homomorphism from $\pi_1(E(V))$ to a finite group G is said to be *proper* if it becomes non-surjective after precomposed with i_{2*}. The G-image is then given by the set of the images of the subgroup $i_{2*}(\mathrm{Ker}(i_{1*}))$ in G under proper homomorphisms.

The computation of the invariants listed above are automated by a software developed by the third author. Before using GPT-5.5, we had already checked all the required equivalences of diagrams in each leaf manually, via Theorem 2.1. Most of them are shown to contain only one equivalence class of handlebody-knots, up to mirror image. Details of such equivalence proofs are contained in the supplementary material [3] where we include both visual proofs via handwritten drawings and certifying files that list the sequence of Reidemeister plus IH moves that connect pairs of diagrams, obtained with the aid of GPT-5.5. The proofs recorded in these certificates generally differ from our earlier manual proofs. All GPT-assisted move sequences included in the supplementary material were independently verified by the authors using the verification code supplied there.

As an exception, there are seven leaves that are shown to contain two equivalence classes. These pairs are $(5_1, 7_{52})$, $(7_{40}, 7_{41})$, $(7_{43}, 7_{44})$, $(7_{59}, 7_{60})$, $(6_{12}, 7_{39})$,

$(7_{64}, 7_{65})$, $(7_{66}, 7_{67})$, each leaf containing handlebody-knots that have the same values of all computed invariants. Here $5_1, 6_{12}$ are taken from the table [10]. Other methods are needed to distinguish them. The situation with the last two pairs $(7_{64}, 7_{65})$, $(7_{66}, 7_{67})$ is relatively simple: Observe $7_{64}, 7_{65}$ (resp. $7_{66}, 7_{67}$) have spines that are 2-sums of the four crossing link L4a1 (resp. the figure eight K4$_1$) and the right and left trefoil knots, respectively. Therefore, by the uniqueness of knotted handle decomposition in [11, Theorem 2.2], if $7_{64}, 7_{65}$ (resp. $7_{66}, 7_{67}$) were equivalent, up to mirror image, then there should exist an orientation-reversing self-homeomorphism of $\mathbb{S}^3$ preserving a tunnel of the link L4a1 (resp. the knot K4$_1$), contradicting [8, Theorem 16.2]; see Fig. 4.1a (resp. Fig. 4.1b). On the other hand,



(a) L4a1 with the tunnel dual to D. (b) K4$_1$ with a tunnel dual to D.

FIGURE 4.1. Neighborhood of the union of L and its tunnel.

[2, Theorem 1.3] classifies handlebody-knots obtained from tangle replacement on the spatial graph G4$_1$ in Fig. 3 ([2] uses $\mathbf{h4_1}$ to denote G4$_1$), and proves $6_{12}, 7_{39}$, $7_{59}, 7_{60}$ are mutually inequivalent, up to mirror image; see [2, Corollary 1.4] for the statement and Figs. 4.2 for an illustration. The inequivalence, up to mirror image, for members in the other three pairs: $(7_{40}, 7_{41})$, $(5_1, 7_{52})$, and $(7_{43}, 7_{44})$, is proved in Section 6. The end result is the union of Tables 1 and 2.

Remark 4.1. The authors have been informed that the pairs $(7_{40}, 7_{41})$, $(7_{43}, 7_{44})$, $(7_{59}, 7_{60})$ can be distinguished by quandle invariants. Ishii and Kishimoto have independently obtained a similar table containing 69 entries, where they find 3 hard pairs. We thank them for communicating these results to us after seeing our table. At the time of writing, we have not had the opportunity to examine their table. Accordingly, based on the information communicated to us, we presume that the two tables contain essentially the same entries.

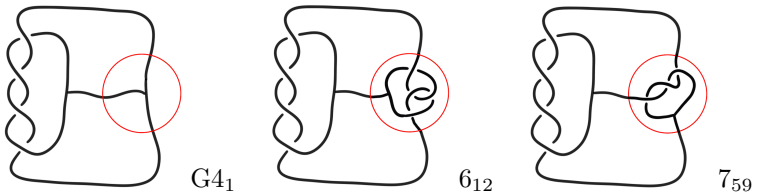


FIGURE 4.2. Tangle replacement on G4$_1$.

The choice of the invariant for each leaf that is not yet considered final is not automated and was manually chosen by the authors. For the initial degenerate tree we selected the Kitano-Suzuki G-invariant with $G = \mathrm{SL}_2(\mathbb{Z}_5)$, which resulted in 54 distinct values and hence 54 new leaves, containing equivalence classes of embeddings with the same value of this invariant. Of these, 28 were considered final. For 23 of these we were able to show mutual equivalence of all handlebodies represented by the diagrams in each by using the Reidemeister moves I through V

(Figures 2.2 and 2.3) and the IH-move (Fig. 2.4), thus obtaining various entries in Table 1.

Four leaves of these 28 only contain nonminimal diagrams. They are manually shown to be nonminimal, as they do not contain any of the portions listed in Figures 3.1-3.3. They happen to be equivalent to three handlebody-knots with six crossings and one with five crossings.

The value 528 of the mentioned Kitano-Suzuki invariant leads to the hard-pair $(6_{12}, 7_{39})$, whereas the values 684 and 724 lead to the two hard-pairs $(7_{43}, 7_{44})$ and $(7_{40}, 7_{41})$.

The remaining 23 leaves of the growing tree $\mathcal{T}$ after the first invariant computation require stronger invariants in order to distinguish inequivalent diagrams. We made here various choices of the invariants: Kitano-Suzuki with $G = S_6$, $\mathrm{SL}_2(\mathbb{Z}_7)$, *G-image* invariant with $G = A_5$ and $G = S_6$, the specific choices being indicated in [19].

To further illustrate the dynamic procedure we list here the sequence of invariants leading to entry 7_{10} in Table 1. The first invariant computed is ks_G, with $G = \mathrm{SL}_2(\mathbb{Z}_5)$ that results in a value of 408 for a large number of diagrams. We further compute on these diagrams the (presumably stronger) invariant ks_G with $G = S_6$ obtaining six distinct values, hence partitioning the already selected diagrams into six distinct invariant-equivalence[2] classes.

Four of these classes happen to contain mutually equivalent diagrams (shown equivalent by using Reidemeister- and IH-moves). We found entries 5_3 and 6_8 in Table 1 of [10] and entries 7_4, 7_{14} in our Table 1. One class contains entries that could be grouped into two sets of mutually equivalent diagrams that were shown to be inequivalent in [2] and named 7_{59}, 7_{60} in Table 1. Finally the class identified by the invariant value of 1272 required the computation of an even stronger invariant. We chose to compute the *G-image* with $G = A_5$, able to separate the diagrams into two classes, each with mutually equivalent diagrams. One class turns out to correspond to entry 6_2 in [10], and the other corresponds to entry 7_{10} in Table 1. We refer to [19] for the complete picture.

5. Irreducibility

To divide the handlebody-knots into Tables 1 and 2, we need to determine their irreducibility. Recall that the *rank* of a handlebody-knot V is the minimal number of generators needed to generate the fundamental group $\pi_1(E(V))$. We use two ways to compute the presentation of $\pi_1(E(V))$: one uses a CW-complex structure of $E(V)$, while the other is the Wirtinger presentation, and then simplify the presentation as much as possible with the software developed by the third author [18]. As a result, we find all except $7_{68}, 7_{69}$ in Table 1 are of rank 3. The ranks of $7_{68}, 7_{69}$ are less than or equal to 4. This allows us to apply the irreducibility test in [5, Corollary 1.3].

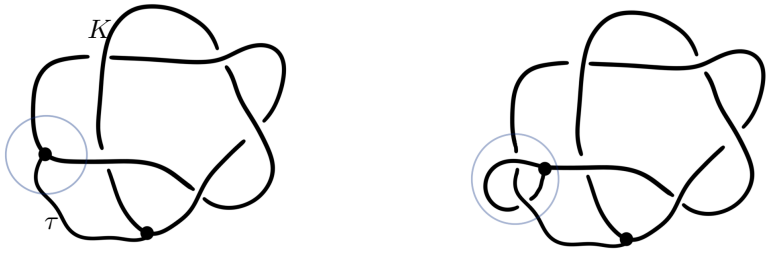
The Kitano-Suzuki invariant ks_G used in the following Theorem is defined in Section 4.1.

Theorem 5.1. *Given a handlebody-knot V with a rank of r and its ks_{A_5}-invariant equal to k_5 and ks_{A_4}-invariant equal to k_4, if*

(i) $r \leq 3$, and k_5 is not congruent to 17 modulo 60, or
(ii) $r \leq 4$, and k_4 is not congruent to 10 modulo 12,

then V is irreducible.

[2]In this case *invariant-equivalent* means diagrams that share the value of both ks_G invariants with $G = \mathrm{SL}_2(\mathbb{Z}_5)$ and $G = S_6$. Note that there is no guarantee that all diagrams in an equivalence class are equivalent as handlebody-knots.



(a) $(5,2)$-torus knot K with tunnel τ. (b) 7_{49}.

FIGURE 5.1. 7_{49} as obtained from tunnel looping.

Proof. By [5, Corollary 1.3], if $r \leq 3$ and $k_5 + 14 \cdot 4 + 19 \cdot 3 + 22 \cdot 5 = k_5 + 223$ is not congruent to 0 modulo 60, then V is irreducible. This implies the first assertion. Again by [5, Corollary 1.3], if $r \leq 4$ and $k_4 + (6 + 16k) \cdot 3 + (2 + 6k) \cdot 4$ is not congruent to 0 modulo $12 + 24k$, $k = 0, 1$, then V is irreducible. In other words, if $k_4 + 26$ and $k_4 + 98$ are, respectively, not congruent to 0 modulo 12 and 36, then V is irreducible. Note that the former implies the latter and hence the second assertion. □

Corollary 5.2. *All handlebody-knots in Table 1 are irreducible.*

Proof. The irreducibility of $7_{68}, 7_{69}$ is detected by Theorem 5.1(ii), and for all the other handlebody-knots except for 7_{49}, their irreducibility is detected by Theorem 5.1(i). For the handlebody-knot 7_{49}, its ks_{A_5}-invariant is 77, and hence the test in Theorem 5.1 fails. We observe, however, that 7_{49} can be obtained by performing a tunnel looping on a tunnel of the $(5,2)$-torus knot [21, Section 6.2]; see Fig. 5.1. Thus, its irreducibility follows from [21, Lemmas 5.1 and 6.3]. □

The value of the ks_{A_5}- and ks_{A_4}-invariants for all handlebodies in Table 1 is included in the supplementary material [3].

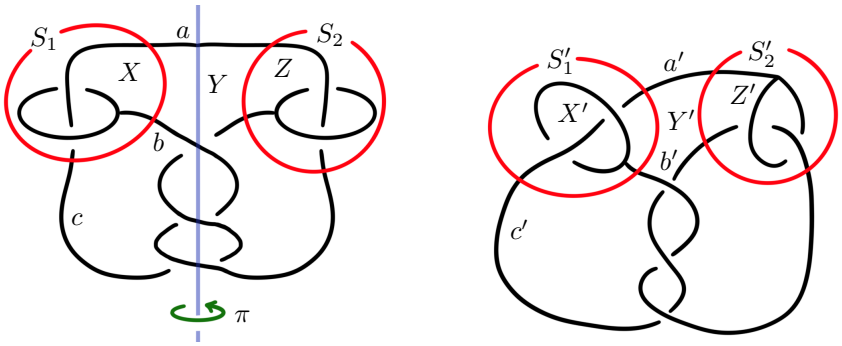
6. Hard pairs

Here we prove the inequivalence of the two handlebody-knots in each of the pairs: $(5_1, 7_{52})$, $(7_{40}, 7_{41})$, $(7_{43}, 7_{44})$. Recall from [11] that a 3-decomposing sphere of a handlebody-knot V is a 2-sphere S meeting V at three disks such that $S \cap E(V)$ is incompressible in $E(V)$. If in addition, the three disks in $S \cap V$ are parallel in V, then S is called a P_3-sphere of V; see [6]. A maximal P_3-system $\mathcal{S}$ is a set $\{S_1, \ldots, S_n\}$ of mutually disjoint P_3-spheres such that the intersections $S_i \cap E(V)$, $i = 1, \ldots, n$, are mutually non-parallel in $E(V)$. By [6, Theorem 1.1], if V admits two maximal P_3-systems $\mathcal{S}, \mathcal{S}'$, then there exists a self-homeomorphism of $(\mathbb{S}^3, V)$ sending $\mathcal{S}$ to $\mathcal{S}'$.

Theorem 6.1. 7_{43}, 7_{44} *are inequivalent up to mirror image.*

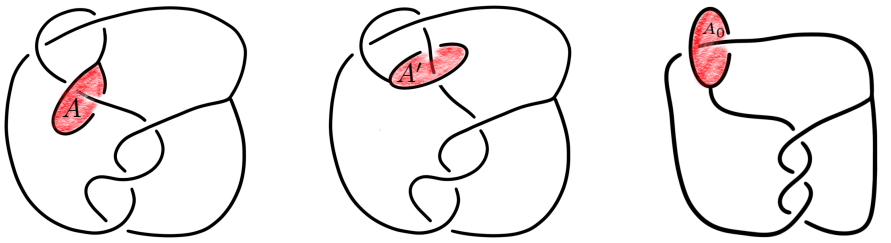
Proof. Denote by V (resp. by V') the handlebody-knot 7_{43} (resp. 7_{44}), and note that the spheres S_1, S_2 (resp. S_1', S_2') in Fig. 6.1a (resp. Fig. 6.1b) both are P_3-spheres. Observe that the union $S_1 \cup S_2$ (resp. $S_1' \cup S_2'$) cuts $\mathbb{S}^3$ into three components X, Y, Z (resp. X', Y', Z') as shown in Fig. 6.1a, (resp. Fig. 6.1b).

Consider the unions $E(X) \cup V$, $E(Y) \cup V$, and $E(Z) \cup V$ (resp. $E(X') \cup V'$, $E(Y') \cup V'$, and $E(Z') \cup V'$), and observe that they are all genus two handlebodies. Additionally, the disks in the intersection $V \cap (S_1 \cup S_2)$ (resp. $V' \cap (S_1' \cup S_2')$) induce a spine for each of them, and hence induce three spatial graphs $\Gamma_X, \Gamma_Y, \Gamma_Z$ (resp. $\Gamma_{X'}, \Gamma_{Y'}, \Gamma_{Z'}$).



(a) P_3-spheres of 7_{43}. (b) P_3-spheres of 7_{44}.

FIGURE 6.1



(a) 7_{40} and annulus A. (b) 7_{41} and annulus A'. (c) 5_1 and annulus A_0.

FIGURE 6.2

The spatial graphs $\Gamma_X, \Gamma_Z, \Gamma_{X'}$, $\Gamma_{Z'}$ are the spatial handcuff graph G2 in Table 3, namely 2_1 in [15], while $\Gamma_Y, \Gamma_{Y'}$ are the mirror image of G3 in Table 3, namely 3_1 in [14], so they are all prime; recall the definition of primeness in Remark 3.2. This implies that $\{S_1, S_2\}$ (resp. $\{S_1', S_2'\}$) is a maximal P_3-system.

Label the arcs in Γ_Y and $\Gamma_{Y'}$ by a, b, c and a', b', c', respectively; see Figs. 6.1a, 6.1b. Then, by the uniqueness of the maximal P_3-system [6, Theorem 1.1] and the fact that there is a self-homeomorphism of $(\mathbb{S}^3, V)$ swapping S_1, S_2 (see Fig. 6.1a), if $7_{43}, 7_{44}$ are equivalent, up to mirror image, there is a homeomorphism $f : (\mathbb{S}^3, V) \to (\mathbb{S}^3, V')$ with $f(S_i) = S_i'$, $i = 1, 2$. In particular, f induces an equivalence g from Γ_Y to $\Gamma_{Y'}$. Obsereve that $X \cap V, Z \cap V$ (resp. $X' \cap V', Z' \cap V'$) each consists of a solid torus and a 3-ball. Since a joins the 3-balls in $X \cap V, Z \cap V$, we have $g(a) = c'$. Similarly, since b joins the solid torus in $X \cap V$ to the 3-ball in $Z \cap V$, we have $g(b) = b'$. Thus, $g(c) = a'$. This contradicts the fact that the constituent knot $b \cup c$ of Γ_Y is a trefoil knot, whereas the constituent knot $b' \cup a'$ of $\Gamma_{Y'}$ is trivial; see G3 in Table 3. □

Theorem 6.2. *7_{40} and 7_{41} are inequivalent up to mirror image.*

Proof. Denote by V, V' the handlebody-knots $7_{40}, 7_{41}$, respectively, and observe that $E(V)$ (resp. $E(V')$) admits an essential annulus A (resp. A') as shown in Fig. 6.2a (resp. 6.2b). Let $\mathcal{N}(A)$ (resp. $\mathcal{N}(A')$) be a regular neighborhood of A in $E(V)$ (resp. A' in $E(V')$). Then the union $V \cup \mathcal{N}(A)$ (resp. $V' \cup \mathcal{N}(A')$) in $\mathbb{S}^3$ is the handlebody-knot 5_1, denoted by V_0; see Fig. 6.2c. By [21, Theorem 1.4], the exterior $E(V_0)$ admits a unique essential annulus A_0.

Claim: A (resp. A') is the unique annulus in $E(V)$ (resp. $E(V')$). Suppose otherwise and $E(V)$ admits an essential annulus A^* non-isotopic to A. By the

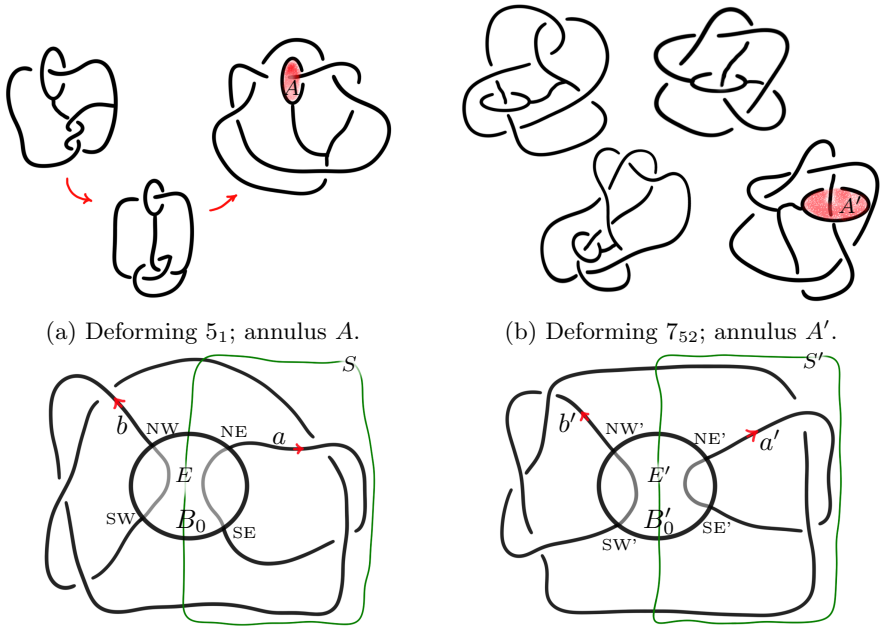
JSJ-decomposition of $E(V)$, if A is not a characteristic annulus, we can take A^* to be a characteristic annulus. Thus, whether A is characteristic or not, A^* can always be isotoped away from A and hence from a regular neighborhood $\mathcal{N}(A)$ of A. In particular, A^* can be regarded as an annulus in the exterior $E(V_0)$, and the incompressibility of $A^* \subset E(V)$ implies that it is incompressible also in $E(V_0)$.

Let A_+, A_- be the components in the frontier of $\mathcal{N}(A) \subset E(V)$. Suppose A^* is ∂-compressible in $E(V_0)$, and D is a ∂-compressing disk. Then, since 5_1 is irreducible, $E(V_0)$ is ∂-irreducible. Therefore compressing A^* along D yields an inessential disk in $E(V_0)$. This, along with the incompressibility of A^*, shows that A^* is ∂-parallel to an annulus A^{**} in ∂V_0. Since A^* is essential in $E(V)$, A^{**} meets $A_+ \cup A_-$. Given ∂A^* does not meet $A_+ \cup A_-$, A^{**} either contains both A_+, A_- or only one of them. If A^{**} contains $A_+ \cup A_-$, then the cores of A_+, A_- are parallel in ∂V_0, so V is disconnected, a contradiction. If A^{**} contains A_+ or A_-, then A^{**} and A_+ or A_- have the same core, and hence A^* is isotopic to A_+ or A_- in $E(V_0)$, and isotopic to A in $E(V)$, a contradiction.

As a result, $A^* \subset E(V_0)$ is ∂-incompressible and hence essential. Since A_0 is the unique essential annulus in $E(V_0)$, A^*, A_0 are isotopic, but A^* is disjoint from $A_+ \cup A_-$, contradicting ∂A_0 cannot be isotoped away from $A_+ \cup A_-$. The same argument applies to V'.

Suppose $7_{40}, 7_{41}$ are equivalent, up to mirror image, and $f : (\mathbb{S}^3, V) \to (\mathbb{S}^3, V')$ is a homeomorphism. Then by the uniqueness of A, A', it may be assumed that $f(A) = A'$ and hence f induces a self-homeomorphism of 5_1 that reverses the orientation of ∂A_0, contradicting that every self-homeomorphism of 5_1 is isotopic to the identity by [20, Theorem 1.2]. □

Theorem 6.3. 5_1 *and* 7_{52} *are inequivalent up to mirror image.*



(a) Deforming 5_1; annulus A.

(b) Deforming 7_{52}; annulus A'.

(c) 5_1: induced tangle.

(d) 7_{52}: induced tangle.

FIGURE 6.3

Proof. Denote by V, V' the handlebody-knots $5_1, 7_{52}$, respectively, and observe that their exteriors $E(V), E(V')$ admit essential annuli A, A' in Figs. 6.3a, 6.3b, respectively. Since $\partial A, \partial A'$ both have exactly one component bounding a non-separating disk in V, V', respectively, $A \subset E(V), A' \subset E(V')$ are the unique essential annulus by [21, Theorem 1.4], up to isotopy. Denote by $D \subset V$ (resp. $D' \subset V'$) the disk bounded by the component of ∂A (resp. $\partial A'$), respectively.

Now, Suppose 5_1 and 7_{52} are equivalent, up to mirror image, and $f : (\mathbb{S}^3, V) \to (\mathbb{S}^3, V')$ is a homeomorphism. Then, by the uniqueness, it may be assumed that $f(A) = A'$, and hence f induces a self-homeomorphism g of $\mathbb{S}^3$ sending $V_A := V \cup \mathcal{N}(A)$ to $V'_A := V' \cup \mathcal{N}(A')$. Let A_a, A_b (resp. A'_a, A'_b) be the two annuli in the frontier of $\mathcal{N}(A) \subset E(V)$ (resp. $\mathcal{N}(A') \subset E(V')$). Then the cores of A_a, A_b (resp. A'_a, A'_b) bound two disks D_a, D_b in V_A (resp. D'_a, D'_b in V'_A).

Cutting V_A (resp. V'_A) along one of D_a, D_b, say D_a, (resp. one of D'_a, D'_b, say D'_a,) gives a regular neighborhood of the right-hand (resp. left-hand) trefoil, while cutting V_A along D_b (resp. V'_A along D'_b) gives a regular neighborhood of a trivial knot. This implies g is orientation-reversing.

Denote by $a, b \subset V_A$ and by $a', b' \subset V'_A$ the arcs dual to D_a, D_b and D'_a, D'_b, respectively. Orient the arcs a, b (resp. a', b') so they point away from D (resp. D'); see Fig. 6.3c (resp. 6.3d). In particular, the union $a \cup b$ (resp. $a' \cup b'$) can be regarded as a 2-string tangle in the exterior B of a regular neighborhood B_0 of $A \cup D$ (resp. the exterior B' of a regular neighborhood B'_0 of $A' \cup D'$). It may be assumed that $g(B_0) = B'_0$. Also, by our choice of orientation and D_a, D_b, D'_a, D'_b, we have $g(a) = a', g(b) = b'$ with the orientation of a, a', b, b' respected.

Let NW, NE, SW, SE (resp. NW', NE', SW', SE') be the four boundary points of $a \cup b$ (resp. $a' \cup b'$) as shown in Fig. 6.3c (resp. 6.3d), and observe that there is a 2-sphere $S.S'$ meeting B_0, B'_0 at a disk E, E' and b, b' at two points, respectively; see Figs. 6.3c and 6.3d. Set $m := \partial E, m' := \partial E'$, and choose $l \subset \partial B_0, l' \subset \partial B'_0$ so $m \cup l$ (resp. $m' \cup l'$) separates the four points NW, NE, SW, SE in ∂B_0 (resp. NW', NE', SW', SE' in $\partial B'_0$).

Since $g(a) = a', g(b) = b'$ with their orientation preserved, g restricts to a homeomorphism from B_0 to B'_0 carrying XX to XX', where XX=NW, NE, SW or SE. Consider the rational tangle $t \subset B_0$ with a slope ∞ with respect to m, l; see Fig. 6.3c. In particular, $t \cup a \cup b$ is a composite link with one summand a Hopf link and the other a left-hand trefoil. Then g being a homeomorphism implies $g(t) = t' \subset B'_0$ is rational. Suppose t' has a slope of $\frac{p}{q}$ with respect to m', l'. Then since $L' := g(L) = t' \cup a' \cup b'$ is a link, the two points NE' and SE' are joined by an arc in t', so q is even.

If $q \neq 0$, then L' is a Montesinos link with three tangles T_1, T_2, T_3 with a slope of $-\frac{1}{3}$, $\frac{p}{q}$, $\frac{1}{2}$, respectively; see Fig. 6.3d. In particular, the branched cover along L' is Seifert fibered over a 2-sphere with 3 exceptional fibers, so L' is prime, contradicting L is a composite link. As a result, we have $q = 0$, and hence (B'_0, t') has a slope of ∞ with respect to m', l'.

Orient L, L' using the orientation of $a \cup b, a' \cup b'$, respectively. Then g preserves the orientation of L, L', yet the linking number of both L, L' is 1, contradicting g reverses the orientation of $\mathbb{S}^3$. □

Acknowledgements

The first author is member of the GNAMPA-INdAM. The fourth author gratefully acknowledges the support from NSTC, Taiwan (grant no. 112-2115-M-110 -001 -MY3).

References

[1] G. Bellettini, G. Paolini, M. Paolini, Y.-S. Wang, *A table of n-component handlebody links of genus $n+1$ up to six crossings*, Math. Proc. Camb. Phil. Soc. **174** (2023), 199–223.

[2] G. Bellettini, G. Paolini, M. Paolini, Y.-S. Wang, *Handlebody-knots obtained by tangle replacement*, arXiv:2511.07796v3, submitted for publication.

[3] G. Bellettini, G. Paolini, M. Paolini, Y.-S. Wang, *Supplementary computational material for "A table of genus two handlebody-knots with seven crossings"*, Zenodo, `https://doi.org/10.5281/zenodo.21512666` (2026).

[4] G. Bellettini, M. Paolini, Y.-S. Wang, *A complete invariant for connected surfaces in the 3-sphere*, J. Knot Theory Ramifications **29** (2020), 1–24.

[5] G. Bellettini, M. Paolini, Y.-S. Wang, *Numerical irreducibility criteria for handlebody links*, Topology Appl. **284** (2020), 1–14.

[6] G. Bellettini, M. Paolini, Y.-S. Wang, *Unique 3-decomposition and mapping classes of knotted handlebodies*, Geom. Dedicata **219**(74) (2025).

[7] S. Buoncristiano, *Fragments of Geometric Topology from the Sixties*, Geometry and topology monographs **6**, University of Warwick, Mathematics Institute (2003).

[8] S. Cho, D. McCullough: *The tree of knot tunnels*, Geom. Topol. **13** (2009) 769–815

[9] A. Ishii, *Moves and invariants for knotted handlebodies*, Algebr. Geom. Topol. **8** (2008), 1403–1418.

[10] A. Ishii, K. Kishimoto, H. Moriuchi, M. Suzuki, *A table of genus two handlebody-knots up to six crossings*, J. Knot Theory Ramifications **21** (2012), 1250035 (9 pages).

[11] A. Ishii, K. Kishimoto, M. Ozawa, *Knotted handle decomposing spheres for handlebody-knots*, J. Math. Soc. Japan **67** (2015), 407–417.

[12] T. Kitano, M. Suzuki, *On the number of $SL(2,\mathbb{Z}/p\mathbb{Z})$-representations of knot groups*, J. Knot Theory Ramifications **21** (2012), 1250003.

[13] J. H. Lee, S. Lee, *Inequivalent handlebody-knots with homeomorphic complements*, Algebr. Geom. Topol. **12** (2012), 1059—1079.

[14] H. Moriuchi, *An enumeration of theta-curves with up to seven crossings*, J. Knot Theory Ramifications **18** (2009), 67–197.

[15] H. Moriuchi, *A table of handcuff graphs with up to seven crossings*, OCAMI Studies Vol 1. Knot Theory for Scientific objects (2007) 179–300.

[16] H. Moriuchi, *A table of θ-curves and handcuff graphs with up to seven crossings*, Adv. Stud. Pure Math. Noncommutativity and Singularities: Proceedings of French–Japanese symposia held at IHES in 2006, J.-P. Bourguignon, M. Kotani, Y. Maeda and N. Tose, eds. (Tokyo: Mathematical Society of Japan, 2009), 281–290.

[17] M. Motto, *Inequivalent genus two handlebodies in S^3 with homeomorphic complements*, Topology Appl. **36**(3) (1990), 283–290

[18] M. Paolini, Appcontour. Computer software. Vers. 2.5.8. Apparent contour. (2018) <`git@github.com:appcontour/appcontour.git/`>.

[19] M. Paolini (2024, July 24). *Complete table of handlebody knots of genus 2 up to seven crossings.* `http://dmf.unicatt.it/paolini/handlebodies/`

[20] Y.-S. Wang, *Unknotting annuli and handlebody-knot symmetry*, Topol. Appl. **305**(1) (2022), 107884.

[21] Y.-S. Wang, *JSJ decomposition for handlebody-knots*, J. Math. Soc. Japan **76**(4) (2024), 1049–1085.

[22] H. Whitney, *Congruent graphs and the connectivity of graphs*, Am. J. Math. **54** (1932), 150–168.

[23] E. C. Zeeman, *Seminar on combinatorial topology*, Notes I.H.E.S. and Warwick (1963).

Dipartimento di Scienze Matematiche, Informatiche e Fisiche, via delle Scienze 206, 33100 Udine, Italy and International Centre for Theoretical Physics ICTP, Mathematics Section, 34151 Trieste, Italy
Email address: giovanni.bellettini@uniud.it

Dipartimento di Matematica, Università di Bologna, Piazza di Porta San Donato 5, 40126 Bologna, Italy
Email address: g.paolini@unibo.it

Dipartimento di Matematica e Fisica, Università Cattolica del Sacro Cuore, 25121 Brescia, Italy
Email address: maurizio.paolini@unicatt.it

National Sun Yat-sen University, Kaohsiung, Taiwan
Email address: yisheng@math.nsysu.edu.tw